Fretting Wear Modeling of Cylindrical Line Contact in Plane-Strain Borne by the Finite Element Method

Huaidong Yang
G. W. Woodruff School of Mechanical
Engineering,
Georgia Institute of Technology,
Atlanta, GA 30332
e-mail: yanghuaidong@gatech.edu

Itzhak Green[1]
Fellow ASME
G. W. Woodruff School of Mechanical
Engineering,
Georgia Institute of Technology,
Atlanta, GA 30332
e-mail: green@gatech.edu

This is the first study to develop an empirical formulation to predict fretting wear (volume removal) under frictional conditions for plane-strain line contacts as borne out by the finite element analysis (FEA). The contact is between a deformable half-cylinder rubbing against a deformable flat block. The FEA is guided by detailed physical conceptions, with results that subsequently lead to the methodical modeling of fretting wear. The materials in contact are first set to steel/steel, then to Alloy617/Alloy617, and finally to copper/copper. Various coefficients of friction (COFs) and the Archard Wear Model are applied to the interface. Initially, pure elastic conditions are investigated. The theoretical predictions for the wear volume at the end of the partial slip condition in unidirectional sliding contact agree very well with the FEA results. The empirical formulation for the initial gross slip distance is constructed, again revealing results that are in good agreement with those obtained from the FEA for different materials and for various scales. The Timoshenko beam theory and the tangential loading analysis of a half elastic space are used to approximate the deflection of the half-cylinder and the flat block, respectively. That theory supports well the empirical formulation, matching closely the corresponding FEA results. The empirical formulation of the wear volume for a general cycle under fretting motion is then established. The results are shown to be valid for different materials and various COFs when compared with the FEA results. Finally, plasticity is introduced to the model, shown to cause two phenomena, namely junction growth and larger tangential deformations. Wear is shown to either increase or decrease depending on the combined influences of these two phenomena. [DOI: 10.1115/1.4043074]

1 Introduction

Fretting is a common occurrence in engineering between two contacting bodies when an oscillatory tangential load is compounded with a normal load. It may be caused by vibration, cyclic temperature changes, cyclic loading in gears, bolts, human joints, bearings, etc. Fretting wear and fretting fatigue are two main tribological failure causes. According to the study by Vingsbo and Söderberg [1], fretting can be sorted into stick, mixed stick-slip, and gross slip regimes. Varenberg et al. [2] define a slip index to determine the different fretting regimes. Under a certain normal load, the contact status goes from stick, to partial slip, and gross slip with the increase in the tangential displacement.

Experimental studies of fretting have been done thoroughly. Junction growth, i.e., the increase in the contact area, is found by Tabor [3] and by Parker and Hatch [4]. The fretting wear experiments are done in cylindrical line contacts [5], cross cylindrical contacts [6], and spherical contacts [7]. Ahmadi et al. conduct fretting wear experiments using an Alloy 617 ball loaded against an Alloy flat disk [8]. An Archard wear model is used to quantify the results. Two types of wear regimes with different wear coefficients are found. One regime is running-in with a relative large wear coefficient, and the other regime is steady state with a relative small wear coefficient.

Analytical studies on the fretting wear are relatively scarce due to the complexity arising from the frictional tangential loading. For the tangential loading of a half elastic space, there is a partial slip condition according to the study by Johnson [9]. The information about the local slip distance at the interface, in partial slip conditions, is necessary for the fretting wear analysis. The analytical solution for the local slip distance under a Hertzian pressure with a constant coefficient of friction is recorded for the 3D spherical contact by Popov and Heß [10]. However, the solution for the cylindrical line contact is not available.

Numerical studies have been first performed for normal contacts [11–13]. Green [14] finds theoretically the onset of plasticity in the normal contact between spherical and cylindrical bodies. The first finite element analysis (FEA) work of parallel cylindrical fretting contact is done by Gupta et al. [15]. However, their model consists of a very coarse mesh with only 285 elements, limited by the typical computational means available at that time. Recent numerical fretting analyses utilizing the FEA method with very fine meshes are done between cylindrical and spherical contacts by Yangand Green [16–18]. The evolution of von Mises stress, plastic strain, junction growth, fretting loop, and scars at the interface is recorded. However, these works do not apply a wear model at the interface. Ghosh et al. [19] simulate the fretting wear of a Hertzian line contact in a partial slip. However, the simulation is not supported by an analytical solution, and the evolution of the wear volume with respect to the sliding distance is not thoroughly explained.

This work incorporates a fretting wear model for a 2D plane-strain contact using FEA (ANSYS 17.1) subject to force-controlled loading in the normal direction and displacement-controlled fretting motion in the tangential direction. Various coefficients of friction (COFs) and the Archard wear model are applied at the interface. The FEA results are generalized by normalization and fitted with empirical formulations. The initial gross slip distance is first defined. The Timoshenko beam theory and the tangential loading analysis of a half elastic space are used to approximate the deflection of the half-cylinder and the block, respectively, supporting the empirical
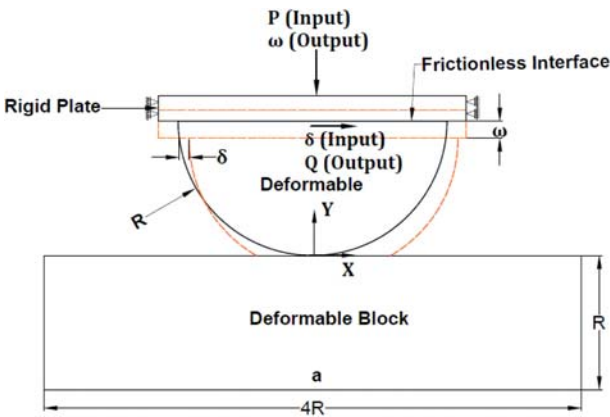
Fig. 1 The loading condition and dimensions of the model

formulation. The wear volume under elastic conditions for a general cycle of the fretting motion is then derived based on the said function of the initial gross slip distance. In conclusion, the effect of plasticity on the wear volume is likewise investigated.

2 Model

The fretting model in this work is shown in Fig. 1. A simulated rigid plate is positioned on the top of a half-cylinder that has a radius of $R = 0.5$ m, which is in contact with an $R \times 4R$ block. The elastic modulus of that plate is set large enough (2×10^{10} GPa) to enforce a uniform downward displacement at the interface between the plate and half-cylinder during the fretting motion. That interface is made frictionless, as the role of the rigid plate is to prevent rotation of the half-cylinder at its upper boundary. The material of the half-cylinder and the flat block is first set to steel/steel, then to Alloy617/Alloy617, and finally to copper/copper. The material properties are listed in Table 1 (see Ref. [21]). Although the Poisson ratios of the chosen materials are very close, the moduli of elasticity and yield strengths are quite distinct.

The fretting loading condition is shown in Fig. 1. X-axis and Y-axis are shown where the origin is located at the initial contact point. For brevity, the positive and the negative directions of X-axis are metaphorically designated as "right" and "left," respectively. The base of the flat block, a, is fixed in both the X and the Y directions (other B.C. will be discussed shortly). A normal force, P, is first applied to the top of the plate, which introduces a vertical interference, ω, designated as the indentation. With the normal force being kept constant, an oscillatory displacement in the X direction δ is applied to the top of the half-cylinder. The oscillation magnitude in each cycle is maintained constant. The fretting cycles obtained are identical to those in Ref. [17], but again for brevity, the schematics are omitted here. The loading condition is displacement controlled in the X direction and force controlled in the Y direction. In other words, the normal load P and the tangential displacement δ are inputs, whereas the interference ω and tangential force Q are outputs.

An Archard wear model, Eq. (1) is used at the contact between the half-cylinder and the block. The wear volume V is proportional to the normal force P and sliding distance S and inversely proportional to the hardness H^2 [12]. The hardness H is assumed to be equal to 2.8*S_y for each material. The dimensionless wear coefficient K, according to the study by Archard and Hirst [20], is typically between 10^{-2} and 10^{-5} for metallic contacts under unlubricated conditions. Without the loss of generality, K is set to

---

10^{-4} in this work.[3] The Archard Wear model is applied locally (i.e., at each nodal point) at the contact region.

$$V = \frac{KPS}{H} \quad (1)$$

2.1 Theoretical Equations for Normal Contact. For normal contact of elastic cylinders in plane-strain, the relations among the load per unit length P/L, the half contact width b, the maximum contact pressure p_0, and the pressure distribution $p(x)$ is given in the following, according to the Hertzian theory of contact [9]:

$$p_0 = \frac{2P}{\pi b L} \quad (2)$$

$$b = \left(\frac{4PR}{\pi L E'}\right)^{1/2} \quad (3)$$

$$p(x) = p_0 \sqrt{1 - \frac{x^2}{b^2}} \quad (4)$$

The symbol ν represents the Poisson ratio, while E' represents the equivalent elastic modulus, which is given by

$$\frac{1}{E'} = \frac{1 - \nu_1^2}{E_1} + \frac{1 - \nu_2^2}{E_2} = \frac{2(1 - \nu^2)}{E} \quad (5)$$

The symbols E_1 and E_2 correspond to the elastic moduli of the half-cylinder and the block, respectively, and ν_1 and ν_2 corresponds to the Poisson ratio of the half-cylinder and the block, respectively. In this work, $E = E_1 = E_2$ and $\nu = \nu_1 = \nu_2$, since the material properties of the two bodies in contact are set to be identical, with the outcome given in Eq. (5).

For the block whose depth equals to the radius of the half-cylinder, $d = R = 0.5$ m, the relation between the interference, ω, and the load per unit length, P/L, is derived by Yang and Green [17]:

$$\omega = \frac{P/L}{2\pi E'} \left\{ 2\ln\left(\frac{2\pi R E'}{P/L}\right) - \frac{1}{1 - \nu} \right\} \quad (6)$$

According to the study by Green [14], the ratio between the maximum contact pressure and the maximum von Mises stress is defined as a parameter, $C = p_0/\sigma_{emax}$. In the elastic contact regime, this parameter is a function of the Poisson's ratio, $C(\nu) = 1.164 + 2.975\nu - 2.906\nu^2$, for $\nu > 0.1938$. By introducing this ratio, the critical half contact width b_c, critical load per unit length P_c/L, and critical interference ω_c, at the onset of plasticity in the contact, are given by Refs. [14] and [17]:

$$b_c = \frac{2RCS_y}{E'} \quad (7)$$

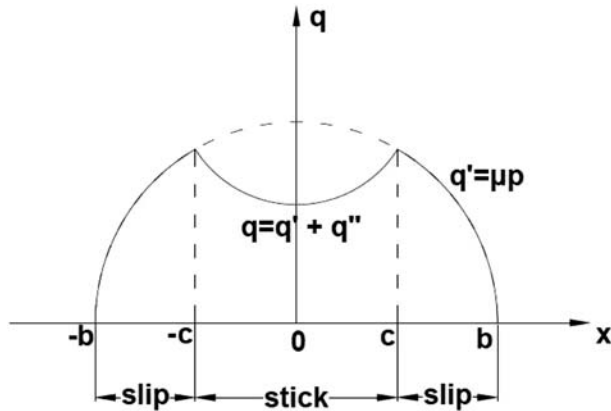$$\frac{P_c}{L} = \frac{\pi R(CS_y)^2}{E'} \quad (8)$$

$$\omega_c = \frac{R}{2}\left(\frac{CS_y}{E'}\right)^2 \left[4\ln\left(\frac{\sqrt{2}E'}{CS_y}\right) - \frac{1}{1 - \nu}\right] \quad (9)$$

By substituting the material properties listed in Table 1 into Eqs. (7)–(9), the critical values are then calculated and listed alongside. The three cases exhibit critical values that are quite distinct, which are nearly an order of magnitude different. The critical values in each case are used to normalize the foregoing results. It is also noted that the oscillation amplitudes in all cases are always maintained at 1*ω_c, which is listed in Table 1.

---

[2]Equation (1) is used here as Archard intended, regarding hardness as a material property. According to the work by Jackson and Green [12], it has been shown that hardness actually depends not only on the yield strength but also on the deformation. For consistency with the Archard original model, however, hardness is used here as if it were a constant material property.

[3]A numerical value for K has to be implemented in the FEA code. However, because of normalization, the results are generalized for any value of K.

Case	Materials	Elastic modulus, E (GPa)	Yielding strength, S_y (MPa)	Poisson ratio, ν	Critical interference, ω_c (μm)	Critical load per unit length, P_c/L (MN/m)	Critical half contact width, b_c (mm)
1	Steel	200	911	0.32	927	38.7	14.9
2	Alloy 617	211	322	0.3	144	4.83	5.26
3	Copper	130	331	0.33	328	7.90	8.30

Fig. 2 The distribution of tangential surface traction of the cylindrical contact under a tangential force, $Q/L < \mu(P/L)$

2.2 Theoretical Equations for Tangential Contact in the Elastic Regime.

Consider the model in Fig. 1 under a Hertzian pressure, $p(x)$ (Eq. (4)), caused by a total normal load per unit length P/L (Eq. (2)). A COF μ is applied to the contact when sliding takes place. According to the study by Johnson [9], when the tangential traction per unit length $Q/L < \mu*(P/L)$, the interface experiences partial slip conditions. As shown schematically in Fig. 2, within the contacting region $(-b < x < b)$, the conditions are stick for $[-c, c]$, and slip between $[-b, -c] \cup [c, b]$. The symbol c is called the stick half-width.

In the slip region, the tangential traction is $q'(x) = \mu p(x)$, where $p(x)$ is the Hertzian pressure given by Eq. (4). If the $q'(x)$ is applied to the entire contact region, $[-b, b]$, there should be another $q''(x)$ to achieve the stick status for $[-c, c]$, where all the points in the stick region displace uniformly. The distributions of $q'(x)$ and $q''(x)$ are given by Johnson [9],

$$q'(x) = \mu p_0 \sqrt{1 - \frac{x^2}{b^2}} \quad -b < x < b \quad (10)$$

$$q''(x) = -\frac{c}{b} \mu p_0 \sqrt{1 - \frac{x^2}{c^2}} \quad -c < x < c \quad (11)$$

Note that $q(x) = q'(x)$ for slip region and $q(x) = q'(x) + q''(x)$ for stick region.[4] Clearly, the flat block and the half-cylinder always experience the tangential traction in opposite directions. For instance, if the half-cylinder is forced to the "right" (i.e., the positive X direction), in the coordinates of this model, the flat block experiences $q'(x)$ and $q''(x)$, whereas the half-cylinder experiences $-q'(x)$ and $-q''(x)$.

When the tangential force per unit length reaches $Q/L = \mu(P/L)$, gross slip starts. In other words, the contact status is slip for the entire range $[-b, b]$, whereas $c = 0$. By taking the two bodies

as two half elastic spaces, the tangential displacement on the surface of contact for each body $\bar{u}(x)$ within contact is given by Johnson [9]:

$$\bar{u}(x) = -\frac{(1-\nu^2)\mu p_0}{bE} x^2 \cdot \text{sgn}(q(x)) + C \quad -b < x < b \quad (12)$$

Hence, in the current coordinates, if the half-cylinder is forced to the "right," the tangential displacement of the half-cylinder $\bar{u}_1(x)$ and that of the block $\bar{u}_2(x)$ are, respectively:

$$\bar{u}_1(x) = \frac{(1-\nu_1^2)\mu p_0}{bE_1} x^2 + C_1 \quad -b < x < b \quad (13)$$

$$\bar{u}_2(x) = -\frac{(1-\nu_2^2)\mu p_0}{bE_2} x^2 + C_2 \quad -b < x < b \quad (14)$$

Consider the boundary condition that at the initial of gross slip $\bar{u}_1(0) = \bar{u}_2(0)$ makes the two constants equal $C_1 = C_2$. The local sliding distance between the half-cylinder and the flat block at the initiation of the gross slip $s_0(x)$ is then derived by $s_0(x) = \bar{u}_1(x) - \bar{u}_2(x)$. By using the relations $E = E_1 = E_2$ and $\nu = \nu_1 = \nu_2$ gives

$$s_0(x) = \frac{2(1-\nu^2)\mu p_0}{bE} x^2 \quad (15)$$

It is again emphasized that this initial gross slip equation is derived for elastic conditions.

3 Mesh Convergence

Mesh convergence has been done to a displacement-controlled model by Yang and Green in Ref. [17]. However, since this model is force controlled in a normal direction and displacement controlled in a tangential direction, it is prudent to verify mesh convergence under such conditions just as well.

Element PLANE183 is used to mesh the model in ANSYS 17.1 (a representative of which is shown in Fig. 3). Taking the case for steel/steel for instance, there are 58,103 elements for the entire model. The size of the refined mesh in the contact area is 8×10^{-4} R. One hundred contact elements (CONTA172 and TARGE169) on each side of the contact are used to simulate the contact between the half-cylinder and the block. Similar mesh schemes are used to model the other two material cases.

A frictionless contact condition is applied to the interface between the rigid plate and the half-cylinder. The contact between the half-cylinder and the flat block is set to frictionless or frictional to investigate different cases. In the frictional contact cases, a small amount of fake slip is generated in the sticking area to calculate the tangential traction in ANSYS 17.1, and it is documented by ANSYS [22]. To alleviate the influence of this fake slip, the elastic slip tolerance factor is used so as to control the fake slip to be smaller than 1% of the sliding distance applied to the top of the half-cylinder.

The results of the mesh convergence for material Case1 (see Table 1) is shown in Table 2. It is first done to the pure normal elastic contact and frictionless loading. To validate the mesh in FEA, the results from ANSYS are compared with those obtained from theoretical predictions. With an input of normal force per
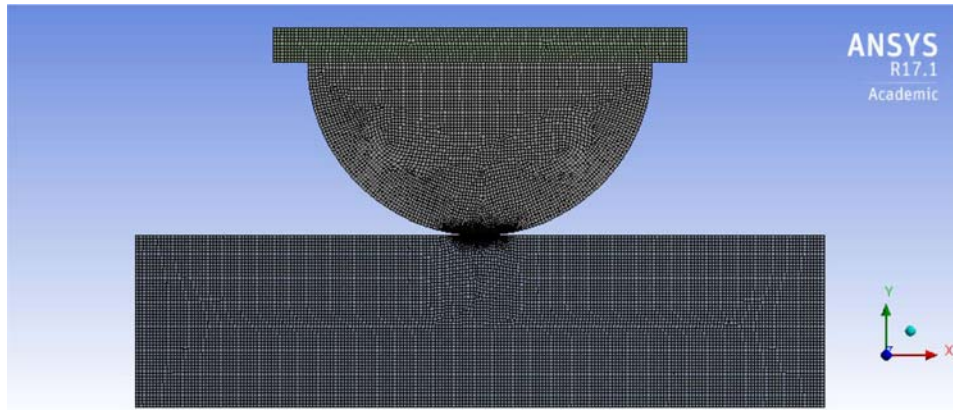
---

[4]Note that $q(x)$ has units of stress and is occurring at the interface. It is distinguished from Q/L, which is the tangential force (per unit length) applied at the top of the half-cylinder, see Fig. 1.

Fig. 3 The model in ANSYS 17.1

Table 2 Comparisons of contact parameters between theoretical predictions and FEA results for material Case1. The relation $\sigma_{emax} = p_0/C$ is according to Green [14]

| Input | | Theoretical predictions | | | | FEA results | | | | | | | |
| | | Equation (6) | Equation (3) | Equation (2) | p_0/C | | | | | | | | |
P^*	P/L (MN/m)	ω (μm)	b (mm)	p_0 (GPa)	σ_{emax} (GPa)	ω (μm)	%dif	b (mm)	%dif	p_0 (GPa)	%dif	σ_{emax} (GPa)	%dif
0.2	7.75	221	6.65	0.741	0.408	222	0.43	6.98	4.91	0.736	−0.72	0.410	0.56
0.6	23.2	590	11.52	1.28	0.706	591	0.13	11.75	2.00	1.28	−0.39	0.718	1.74
1	38.7	927	14.88	1.66	0.912	929	0.24	14.93	0.36	1.65	−0.16	0.930	2.03

unit length P/L (ranges from $0.2*P_c/L$ to $1*P_c/L$), the half contact width b is calculated by Eq. (3), and the interference ω is calculated by Eq. (6). The maximum contact pressure p_0 is then derived by Eq. (2). The maximum von Mises stress $\sigma_{emax} = p_0/C$ is consequently obtained. The theoretical results for Case1 are compared with those from the finite element method (ANSYS 17.1), as listed in Table 2. The percentage differences are listed under "%dif" for each of the parameters. Except for the difference of half contact width b, i.e., 4.91% under $0.2\ P_c$ due to the relative coarse mesh, all the other differences are below 3%. Table 3 lists the results for the case of $P^* = 1$, but for frictional loading with $\mu = 0.3$, for material Case 1. The half contact width converges to 15.2 mm after the mesh size is reduced to 0.8 mm and below (this is relative to the cylindrical radius of 500 mm). Note (Table 2) that the theoretical value for the half contact width is 14.88 mm for frictionless contact. Clearly, further refinement of the mesh is unnecessary,

Table 3 The half contact width for different mesh sizes in the contact region for a normal load, $P^* = 1$, with elastic-perfectly plastic model for material Case 1

Mesh size in contact region (mm)	8	4	2	0.8	0.4
Half contact width (mm)	16.0	15.7	14.5	15.2	15.2

and thus, the mesh size of 0.4 mm is mostly adopted. In addition, the region of contact is safeguarded to always be confined within the refined mesh. Similar mesh convergence processes for the other two material cases have also been done with similar outcomes. Therefore, the mesh can be regarded established for the elastic normal contact.

Now, mesh convergence verification is done also for tangential loading. Under a tangential loading per unit length $Q/L < \mu^*(P/L)$,
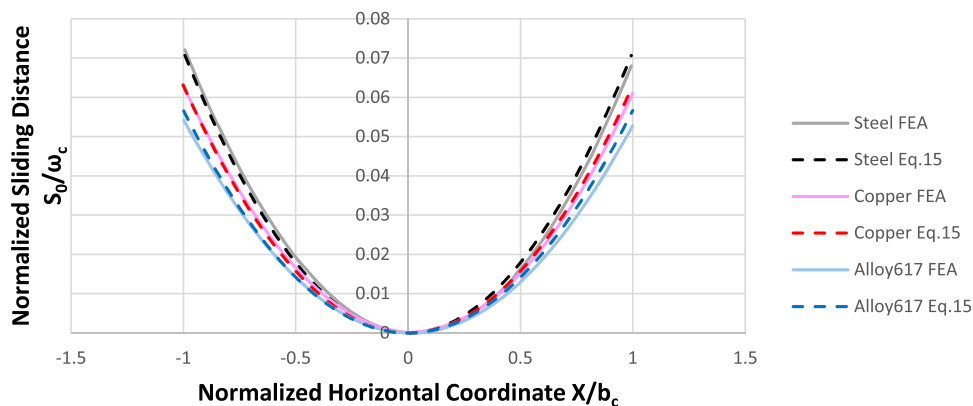

Fig. 4 The normalized sliding distance at inception of gross slip under $P^* = 1$ with $\mu = 0.3$ for three material cases

the contact status is partial slip. At the inception of gross slip, the relative slip distribution (for the situation when the half-cylinder is forced to the right), $s_0(x)$, is given by Eq. (15). That theoretical result is compared with those obtained by FEA.

Figure 4 shows the normalized local sliding distance under $P^* = 1$ with $\mu = 0.3$ at the inception of the gross slip for different pairs of materials. By inputting the normal load per unit length P_c/L, the maximum contact pressure p_0 and the half contact width b are obtained by Eqs. (2) and (3). With the known parameters, p_0, b, E, ν, and μ, the sliding distance $s_0(x)$ is derived by Eq. (15) and normalized by the critical interference ω_c. In the FEA model, $P^* = 1$ is first applied to the top rigid plate and then $1*\omega_c$ sliding distance to the "right" is stepwise applied to the top of the half-cylinder (see the stepwise details in Ref. [22]). By investigating the contact status during sliding, the gross slip starts at the sliding distance of $0.44*\omega_c$. The local sliding distance $s_0(x)$ at $0.44*\omega_c$ is then obtained from ANSYS 17.1 as the local sliding distance at inception of the gross slip. The theoretical prediction agrees very well with the FEA results with a maximum difference less than 5% at the edges of the contact for all three cases. Note that Eq. (15) shows symmetry with respect to x, and the FEA results confirm that behavior. The good agreement also exists for other material cases with different normal loads and different COFs, but for brevity, those results are omitted. With that verification, it is concluded that the mesh
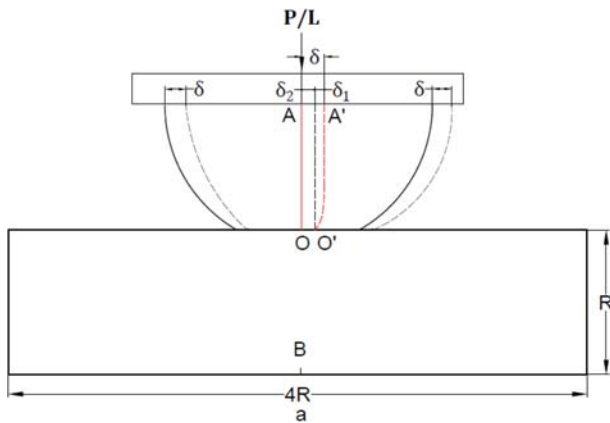
convergence for elastic contacts is likewise established for tangential loading just as well.

Note that since there is no closed-form solution for elastic–plastic contacts under the combination of normal and tangential loads, the elements of the mesh are iteratively refined by a factor of two until there is a less than 1% difference in the contact width between the iterations.

4 Results and Discussion

4.1 The Initial Gross Slip Distance. In the model of this work, after the normal load P/L is applied, the sliding distance δ is applied uniformly to every point on the top of the half-cylinder, as shown in Fig. 5. Before gross slip initiates, the sliding distance δ equals to the addition of the deflection of the half-cylinder δ_1 and the tangential displacement of the stick region δ_2, while the centerline of the half-cylinder OA deforms to $O'A'$. The deflection of the half-cylinder δ_1 equals to the deflection of the centerline. The midpoint of the contact region is point O, which is also the last point in stick just before the gross slip starts. The tangential displacement of the stick region δ_2 equals to the tangential displacement of the midpoint O to O', so $\delta_2 = \overline{OO'}$.

For the frictional contact under the partial slip condition, as the sliding distance δ increases, the tangential traction Q/L increases with it. When $Q/L = \mu(P/L)$, the onset of the gross slip begins. The corresponding sliding distance is designated to the initial gross slip distance δ_i. That δ_i varies under different P/L and different COFs. Figure 6 shows both the FEA results and theoretical predictions for the evolutions of the normalized initial gross slip distance δ_i/ω_c with different P^* and μ for steel/steel. The inset of the figure shows the same results but in linear scale coordinates. The δ_i is shown to be proportional to P/L and μ. A fitting function is found to express δ_i analytically as follows:

$$\delta_i = 4.78\mu^{1.15}\left(\frac{P/L}{RE}\right)^{0.928} R \qquad (16)$$

The rationale for this fit form is forthcoming (details are provided also in the Appendix).

The predicted normalized initial gross slip distance from the fitting function in Eq. (16) is compared with the results from the FEA, as shown in a semi-log scale shown in Fig. 6. The normalized load is given in the log scale to spread the data points at low P^*. The results from the FEA and the fitted function agree well

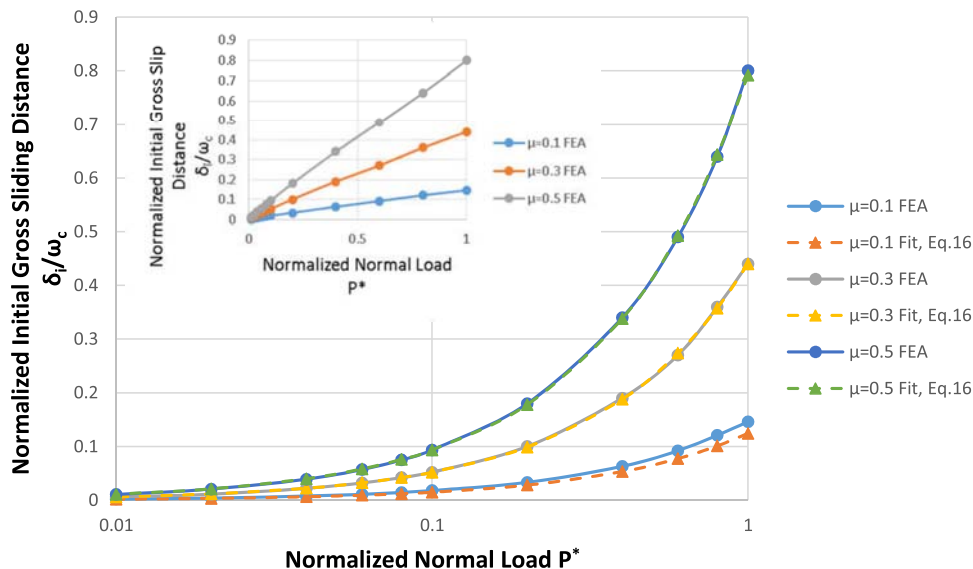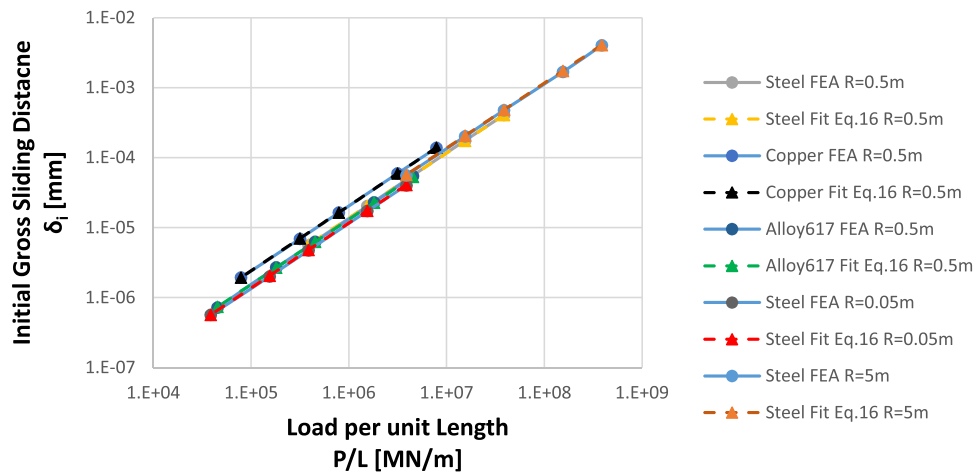**Fig. 5 The schematic of the sliding distance**

Fig. 6 The normalized initial gross slip distance under different normalized normal loads with different COFs for the FEA results and fitting functions, Eq. (16), for steel/steel

Fig. 7 The dimensional initial gross slip distance under different normal loads with $\mu = 0.3$ for the FEA results and fitting functions results for steel/steel (for $R = 0.05$ m, 0.5 m, and 5 m), for Alloy617/Alloy617, and for Cu/Cu (for $R = 0.5$ m)

with the maximum difference of less than 5%. Noteworthy, Fig. 7 shows the dimensional initial gross slip distance under $\mu = 0.3$ and different normal loads for three different pairs of material for $R = 0.5$ m and for steel/steel also for three radii $R = 0.05$ m, 0.5 m, and 5 m. The normal load for each material ranges from $0.01*P_c/L$ to $1*P_c/L$. While the three materials listed in Table 1 are vastly different in their properties, the results from the FEA and the fitted function agree well with less than 5% difference even when the radii are orders of magnitude different. Therefore, in the foregoing analysis, Eq. (16) is used to predict the initial gross slip distance.

The initial gross slip δ_i as given by Eq. (16) seems nearly linearly proportional to μ and P/L. This is explained in the Appendix with the Timoshenko beam theory and half elastic space loading analysis. The deflection of the half-cylinder δ_{i1}, where the gross slip initiates, is obtained in the Appendix, specifically see Eq. (A8). By nullifying the unknown but small moment on the tips, $M_0/L = 0$, the deflection of the half-cylinder can be estimated.
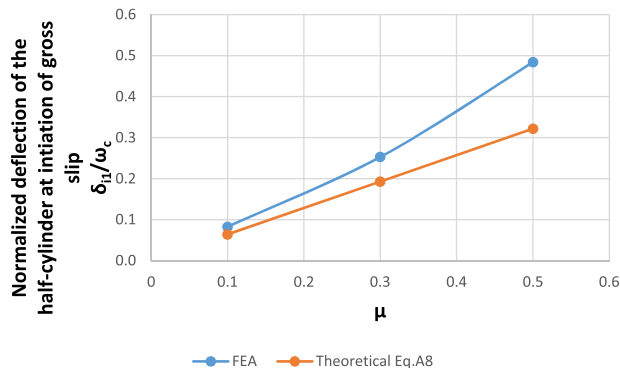
Figure 8 shows the deflections of the half-cylinder at the initiation of gross slip from FEA and Eq. (A8) (with M_0/L being neglected as discussed in the Appendix), for $P^* = 1$ at three different COFs. Although the results from both seem to converge for small COFs, the difference increases with the COFs, which causes larger tangential loads and strains. Recall that the strain-displacement relation in the Timoshenko beam analysis is valid for small strains. Consequently, this is the cause for the discrepancy.

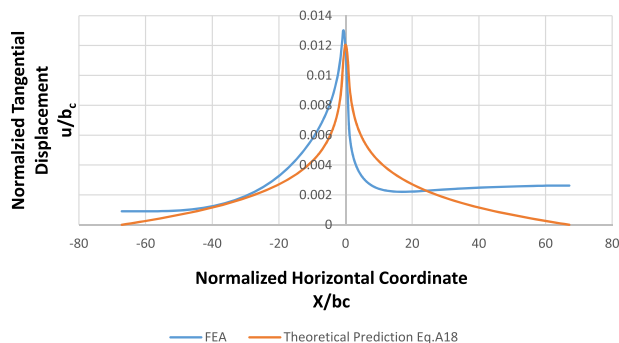The tangential displacement δ_{i2} can be estimated by taking the block as a half elastic space and applying the Hertzian distributed tangential traction to the contacting region. The tangential displacement distribution $u(x)$ on the surface is derived by Eq. (A18). Figure 9 shows the $u(x)$ from FEA and Eq. (A18) at $P^* = 1$ with $\mu = 0.3$. The results agree well on the "left" side of the surface with little difference at the contact center. A larger difference appears on the "right" side, since the boundary condition of the right side of the block is free, so the block does not produce sufficient resistance to horizontal deflection. The difference is likewise heightened by ignoring the normal load, $p(x)$, when calculating $u(x)$. Fortunately, however, the tangential displacement δ_{i2} is relevant only on the "left" part ($x < 0$) of the surface anyhow. Therefore, the estimation in Eq. (A19) is unaffected by the differences shown in the behavior on the "right" side. Noteworthy, Eqs. (A8) and (A19) that estimate δ_{i1} and δ_{i2}, respectively, are nearly linearly proportional to μ and P/L, which provides the rationale for Eq. (16). The slight deviation from linearity is caused by the difference in the boundary conditions used in the FEA pitted against the half-space assumption used in the analytical model.

4.2 The Wear Volume at Initiation of Gross Sliding.
As discussed in Sec. 2.2, before gross sliding starts, the contact condition is partial slip and partial stick, as shown in Fig. 2. The local Archard Wear model is applied to the interface, as given by the following equation:

$$v(x) = \frac{K}{H} p(x) s(x) \qquad (17)$$

Fig. 8 The deflections of the half-cylinder at the initiation of the gross slip from FEA and Eq. (A8) with for $P^* = 1$ at different COFs

Fig. 9 The tangential displacement on the surface of the block at $P^* = 1$ with $\mu = 0.3$ from FEA and half elastic space estimation

Here, only the wear on the half-cylinder is considered. The local wear volume $v(x)$ is proportional to the dimensionless wear coefficient K, contact pressure $p(x)$, and the local sliding distance $s(x)$, whereas it is inversely proportional to the hardness H. Clearly, wear happens in both the half-cylinder and the block, in which case the wear volume is just twice that of the case for the half-cylinder alone. This is true for identical materials in contact. Had the materials been different, the wear volume would be inversely proportional to the hardness. Note that the evolution of the contacting profile due to wear is not considered here.

At the initiation of gross sliding, the local sliding distance is $s(x) = s_0(x)$, as given by Eq. (15). The pressure distribution can be approximated by the Hertzian pressure $p(x)$ as given by Eq. (4). The total wear volume at the initiation of gross sliding V_0 can be derived by integrating Eq. (17) over the region in contact:

$$V_0 = \int_{-b}^{b} \frac{K}{H} p(x)s_0(x)dx = \int_{-b}^{b} \frac{K}{H} p_0 \sqrt{1 - \frac{x^2}{b^2}} \frac{2(1-\nu^2)\mu p_0}{bE} dx \quad (18)$$

The result of the Eq. (18) gives the wear volume at the initiation of gross slip, giving:

$$V_0 = \frac{(1-\nu^2)\mu \pi K p_0^2 b^2}{4HE} \quad (19)$$

To normalize the results, the critical wear volume V_c is defined as follows:

$$V_c = \frac{K_c \omega_c (P_c/L)}{H} \quad (20)$$

Herein, the critical wear coefficient is defined as follows: $K_c = 1$.

Figure 10 shows the normalized wear volume at the initiation of gross slip V_0/V_c from FEA and Eq. (19) at different normal loads and COFs for steel/steel. Since the tangential displacement is applied stepwise, it is hard to pinpoint numerically the initiation of gross slip. Conversely, the two steps changing from partial slip to gross slip are easy to detect. Thus, V_0 in the FEA is decided as the average volume between these two steps. As shown in Fig. 10, the results in the FEA and from Eq. (19) agree very well with less than 5% difference, which further verifies the theoretical prediction.

Figure 11 shows the wear volume at the initiation of gross slip V_0 from FEA and Eq. (19) with $\mu = 0.3$ now for different material pairs. The normal load for each material ranges from $0.01*P_c/L$ to $1*P_c/L$. The results for the three cases from the FEA and Eq. (19) are all in

excellent agreement with less than 5% difference, which supports the viability of using Eq. (19) for different material pairs.

4.3 Prediction of Fretting Wear Volume Under Elastic Conditions. During the fretting motion, the amplitude of each cycle in different cases (see Table 1) is maintained at $1*\omega_c$. Figure 12 shows the typical evolution of wear volume during one cycle of the motion from FEA results at $P* = 1$ with different COFs for steel/steel under elastic conditions. The nominal sliding distance, S_n, represents the cumulative tangential sliding distance applied to the top surface of the half-cylinder, which is different from the local sliding distance at the contact region. It is also different from δ, which is the tangential displacement applied to the top surface of the half-cylinder. For $\mu = 0$, the wear volume increases linearly with respect to the nominal sliding distance, and it is a special case for gross slip fretting. For $\mu = 0.3$, there are two parts in each direction of sliding (the half-cylinder changes direction at $S_n* = S_n/\omega_c = 1$, 3, etc.). At the beginning, the contact status is partial slip, and the wear volume increases slowly. As the half-cylinder displaces further, gross slip starts and the wear volume increases linearly at the same rate as that in the case of $\mu = 0$. For $\mu = 1$, the contact status is always partial slip with no gross slip. Thus, the wear volume is negligible compared with the other two cases. In this study, the prediction of the wear volume is only done for the case when the gross slip condition is reached.

For the case with $\mu = 0.3$ as shown in Fig. 12, the evolution of the wear volume is periodic after $S_n* = 1$. Hence, a general cycle is presented in the figure, starting where the half-cylinder is positioned at the rightmost point, i.e., $x* = 1$ or $S_n* = 1$, heading back to the leftmost position, i.e., $x* = -1$ or $S_n* = 5$, thus completing a general cycle. Then, the half-cylinder changes motion returning to the rightmost position.

Thus, the wear volume for a general cycle is analyzed by taking the cycle, $S_n* = 1$ to 5, for instance. At the beginning of the cycle ($S_n* = 1$), the half-cylinder is at the rightmost position, $x* = 1$. Since the half-cylinder is forced to the right before reaching $S_n* = 1$, its centerline is predeflected by a tangential force acting to the right. At the beginning of the cycle, the half-cylinder starts to move to the left. The centerline of the half-cylinder now restores and deforms from the right to the left. As a result, it takes a nominal sliding distance $2\delta_i$ (i.e., $S_n = 2\delta_i$) to finish the partial slip condition, with a corresponding wear volume that is $V = 2V_0$. As the half-cylinder slides further to the left, gross slip starts, i.e., the nominal sliding distance equals to the sliding distance in the contact region, $s(x) = \Delta S_n$. The normalized wear rate, i.e., the slop
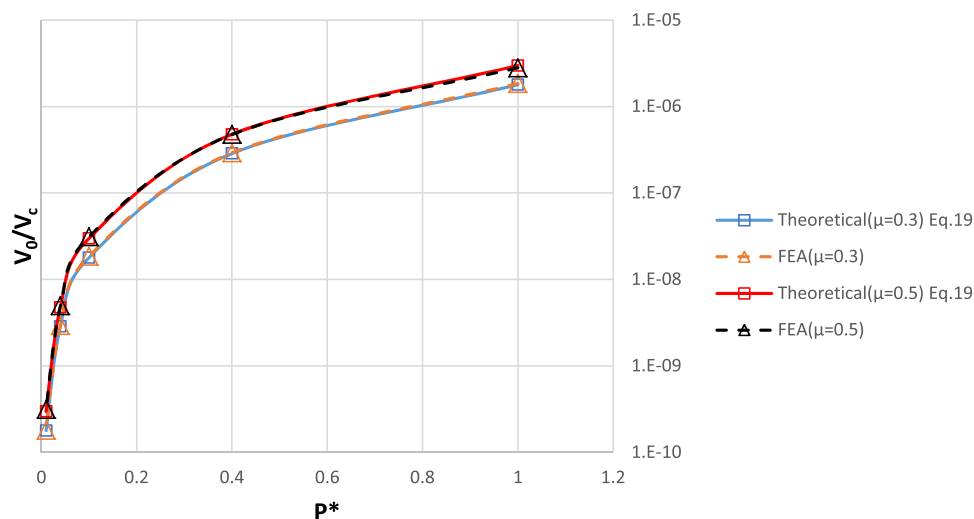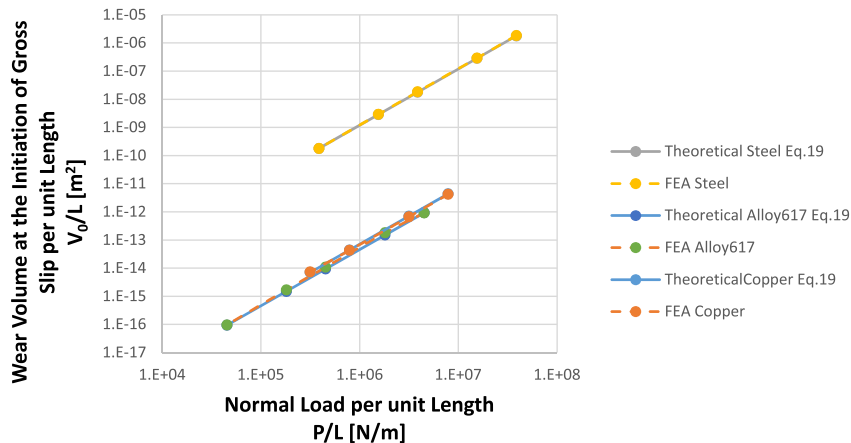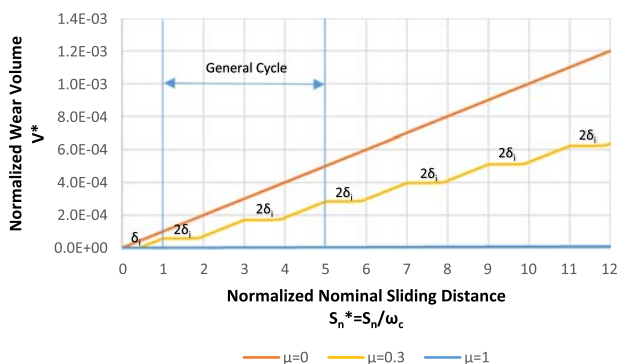

Fig. 10 The normalized wear volume at the initiation of the gross slip, V_0/V_c, from FEA and Eq. (19) at different normal loads and COFs with $K = 10^{-4}$ for steel/steel

Fig. 11 The normalized wear volume at the initiation of gross slip, V_0/V_c, from FEA and Eq. (19) at different normal loads with $\mu = 0.3$ for steel/steel, Alloy617/Alloy617, and copper/copper

Fig. 12 The FEA results of the evolution of normalized wear volume during three cycles of fretting motion at $P^* = 1$ for steel/steel in elastic contact

of the normalized wear volume in Fig. 12, for the gross slip is

$$\frac{\Delta V^*}{\Delta S_n^*} = \frac{\int_{-b}^{b} \frac{Kp_0(x)\Delta S_n dx}{H} / \frac{KP_c\omega_c}{H}}{\Delta S_n/\omega_c} = K\frac{\int_{-b}^{b} p_0(x)dx}{P_c} = KP^* \quad (21)$$

Here, $\Delta V^* = \Delta V/V_c$, $\Delta S_n^* = \Delta S_n^*/\omega_c$.

When the half-cylinder returns back to the right at $x^* = 0$ or $S_n^* = 3$, the second partial slip starts with $V = 2V_0$. After that, another gross slip begins with the normalized wear rate given by Eq. (21). Thus, the total wear volume for a general cycle during the partial slip condition is as follows:

$$V_{partial}^* = 4V_0^* \quad \delta_i^* < 0.5 \quad (22)$$

The total normalized nominal sliding distance for the gross slip condition during a general cycle is $\Delta S_n^* = 4(1 - \delta_i^*)$. Then, the total wear volume for the gross slip condition during a general cycle is

$$V_{slip}^* = \Delta S^* \frac{\Delta V^*}{\Delta S^*} = 4(1 - \delta_i^*)KP^* \quad \delta_i^* < 0.5 \quad (23)$$

The normalized wear volume for a general cycle of the fretting motion is then the sum of $V_{partial}^*$ and V_{slip}^*:

$$V^* = 4V_0^* + 4(1 - \delta_i^*)KP^* \quad \delta_i^* < 0.5 \quad (24)$$

If $\delta_i^* > 0.5$, the partial slip condition will last for the whole cycle, which leads to a very small (negligible) wear volume.

Figure 13 shows the normalized wear volume for a general cycle of fretting motion under elastic condition with different normal loads and COFs for steel/steel. The results from FEA and Eq. (24) agree very well, which further verifies the theoretical predictions. For the case with $\mu = 0.5$, the wear volume first increases with the normal load as predicted by the Archard Wear model. However, the wear
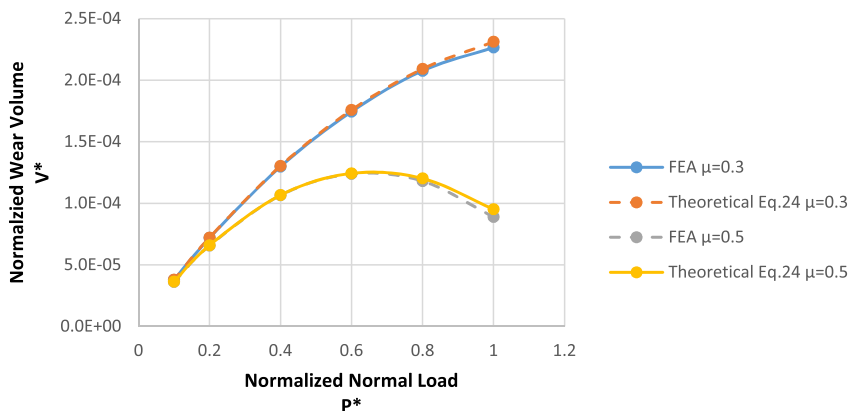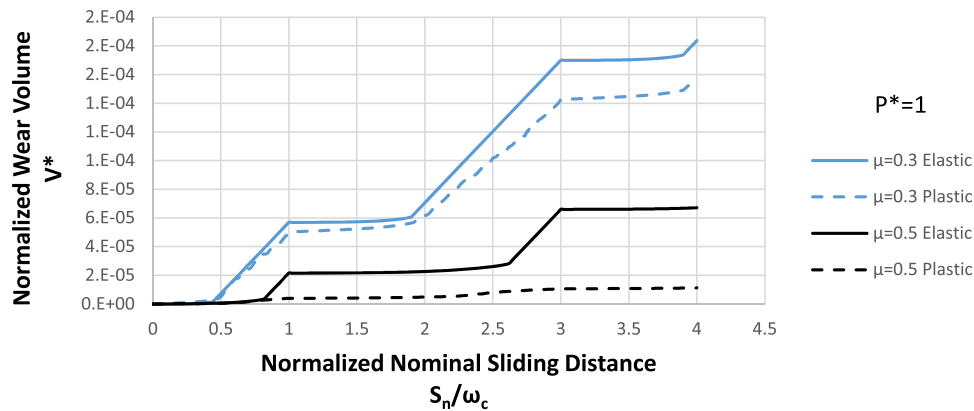

Fig. 13 The wear volume for a general cycle of fretting motion at elastic condition for different normal loads and COFs, comparing FEA and theoretical predictions for steel/steel (for $R = 0.5$ m)
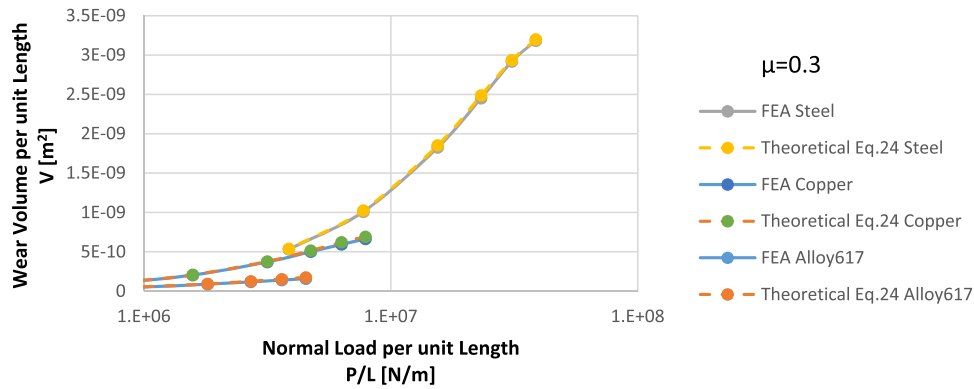
Fig. 14 The wear volume for a general cycle of fretting motion at elastic condition with $\mu = 0.3$ under different normal loads from FEA and theoretical predictions for steel/steel, Alloy617/Alloy617, and copper/copper (for $R = 0.5$ m)

Fig. 15 The evolution of wear volume at elastic and plastic conditions with different COFs under $P^* = 1$ for steel/steel during one cycle of fretting motion (for $R = 0.5$ m).

volume decreases as the normal load further increases, because δ_i^* increases with P^*, which then decreases V^*, as shown in Eq. (24).

Figure 14 shows the results of the wear volume for a general cycle of fretting motion under elastic condition with $\mu = 0.3$ under different normal loads, now for three different material cases (see Table 1). The results from the FEA and theory are in very good agreement, which further verifies the analytical predictions.

4.4 The Effect of Plasticity. In the previous section, the wear volume is considered for elastic conditions. Here, the elastic-perfectly plastic contact model is applied. To find the influence of plasticity on the wear volume, two groups of loading conditions are compared. One is the loading that introduces plasticity, and the other is the same loading but yielding (or plasticity) is disabled (i.e., pure elasticity is open endedly imposed on the material in ANSYS 17.1, as it is solved in Sec. 4.3). The wear volumes between the elastic and plastic conditions are then compared in Fig. 15. Figure 15 shows the evolution of the wear volume at $P^* = 1$ with different COFs under elastic and elastoplastic conditions. Plasticity appears due to the combined effects of normal and the frictional tangential loadings. The wear volumes under pure elastic conditions are larger than those under elastoplastic conditions in these two cases. For $\mu = 0.3$, there is a larger tangential deflection in the elastoplastic case, which decreases the gross slip distance and the wear rate during gross slip. Consequently, the wear volume in the elastoplastic case is smaller. For $\mu = 0.5$, the decrease of the wear volume in the elastoplastic condition is dominated by the junction growth effect (see details in Ref. [17]). Due to the large COF, higher plastic strains (deformations) are generated at the interface, causing an increase of the contact region, i.e., causing junction growth. The junction growth leads to the partial slip condition at the two limit positions during the fretting motion, which greatly decreases the wear volume.

It should be noted that the wear volumes in elastic cases are not always larger than those in elastoplastic cases under the same loading conditions. As shown in Fig. 16, the wear volume at $P^* = 3$ with $\mu = 0.3$ is larger in the elastic case first, but larger in the elastoplastic case after three-fourth of the cycle that keeps getting larger up to three cycles, which is the largest number of the cycle in the current simulation. Wear is larger in the elastic case first, because plasticity introduces the junction growth, which decreases the sliding distance at the interface with the same amount of nominal sliding distance. It is larger in the elastoplastic case afterward because the cross section $A(x)$ given in Eq. (A3) is getting larger in the elastoplastic contact, which decreases the deflection. Consequently, the sliding distance at the interface is larger in the elasto-plastic case than that in the elastic case after one cycle.

5 Conclusion

A fretting wear model is presented in this work for a cylindrical line contact, under 2D plane-strain conditions, for force controlled in the normal direction and displacement controlled in the tangential direction. Friction and the Archard wear model are applied at the interface. Three different material pairs are examined by the model. The following are the outcomes:

(1) The initial gross slip distance is defined and approximated with the Timoshenko beam theory and line loading of a half elastic space. A fitting function for the initial gross sliding distance is also derived. Both the theoretical
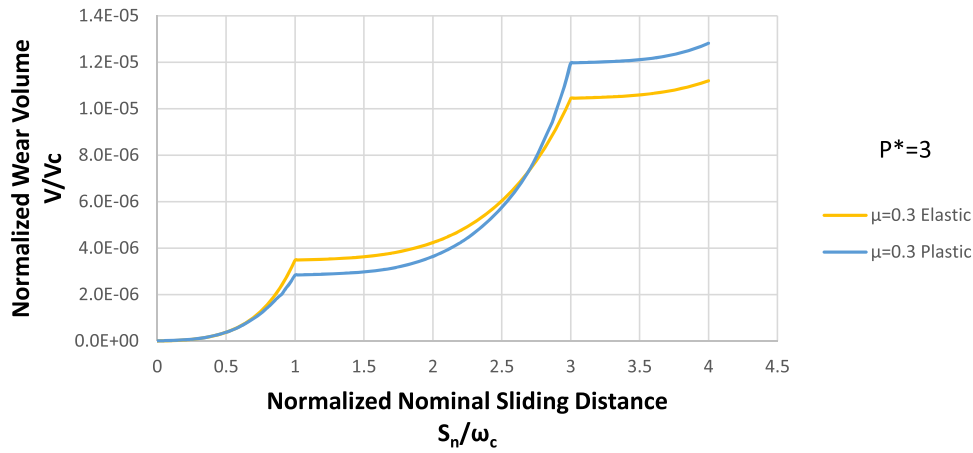
Fig. 16 The evolution of wear volume at elastic and plastic conditions with $\mu = 0.3$ under $P^* = 3$ for steel/steel during one cycle of fretting motion

approximation and the fitting function agree well with the FEA results.

(2) The wear volume at the initiation of the gross slip is derived. Results between the theoretical prediction and FEA are in good agreement.

(3) The wear volume under elastic conditions for a general cycle of the fretting motion is derived based on the fitting function of the initial gross sliding distance. The results are in good agreement between the theoretical predictions and the FEA.

(4) The effect of the plasticity is analyzed. On the one hand, under small normal loads, plasticity introduces small deflections and junction growth when COFs are large. These two effects decrease the wear volume. On the other hand, under larger normal loads, plasticity introduces larger cross sections, which makes the two bodies stiffer to the tangential load. As a result, the deflection decreases, and the wear volume increases.

Acknowledgment

Nomenclature

b = half contact width
c = stick half contact width
q = tangential traction, $q = q' + q''$
s = local sliding distance
v = local wear volume
A = cross section of the beam
C = Poisson's ratio parameter
E = elastic modulus
G = shear modulus
H = material hardness
I = second moment of area
K = dimensionless wear coefficient
L = transverse length along the cylindrical contact
R = radius of half-cylinder
V = wear volume
$\bar{u}$ = tangential displacement on the surface of a half elastic space
b_c = critical half contact width
p_0 = maximum contact pressure
p_{0c} = critical maximum contact pressure
s_0 = local sliding distance at the initiation of the gross slip
E_1 = elastic modulus of the half-cylinder

E_2 = elastic modulus of the block
S_n = nominal sliding distance
S_y = yield strength
V_0 = wear volume at the initiation of the gross slip
V_c = critical wear volume
q' = tangential traction at slip region, $\mu p(x)$
q'' = supplementary tangential traction at stick region
E' = equivalent elastic modulus
P^* = normalized normal force, P/P_c
V^* = normalized wear volume, V/V_c
S_n^* = normalized nominal sliding distance, S_n/ω_c
M_0/L = moment on the tip of the half-cylinder per unit length
P/L = normal force per unit length
P_c/L = critical normal force per unit length
Q/L = tangential force per unit length
δ = horizontal displacement
δ_i = initial gross slip distance
δ_{i1} = the deflection of the half-cylinder at the initiation of the gross slip
δ_{i2} = the displacement of the stick region at the initiation of the gross slip
δ^* = normalized horizontal displacement, δ/ω_c
Δ = the deflection of the half-cylinder
μ = coefficient of friction
ν_1 = Poisson's ratio of the half-cylinder
ν_2 = Poisson's ratio of the block
φ = angle of the mid-surface of beam
ω = interference
ω_c = critical interference
ω^* = normalized interference, ω/ω_c

Appendix

The initial gross sliding distance for elastic contacts can be estimated by regarding the half-cylinder as a Timoshenko beam[5] while assuming the block as a half elastic space. The loading condition of the half-cylinder is shown in Fig. 17, when the gross slip initiates, i.e., when $Q/L = \mu(P/L)$. In addition to Q/L, there is also a moment per unit length M_0/L, acting about the tip of the half-cylinder. This moment M_0/L is caused by the curvature of the contacting surface and the local tangential traction $\mu p(x)$ (as shown in Fig. 17(b)). This moment is directly related to μ and P/L. The moment distribution $M(x)/L$, the second moment of area $I(x)/L$, and the

---

[5]The Timoshenko beam is appropriate for thick or short beams, since it accounts for shear deformation and rotational bending effects.
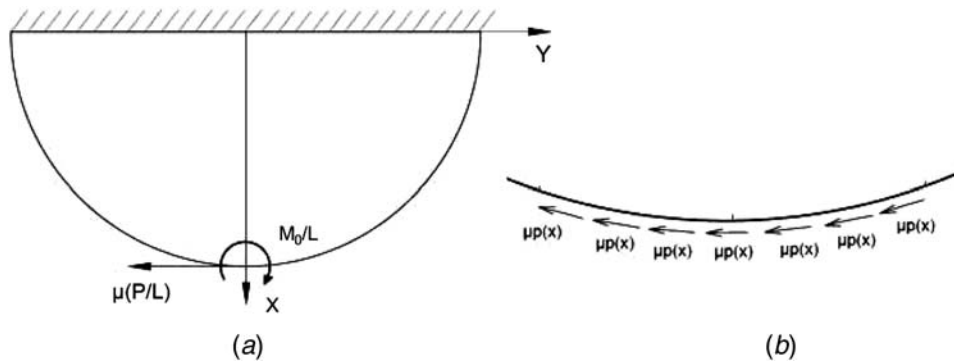
Fig. 17 (a) The loading condition of the half-cylinder as a Timoshenko beam at slip onset and (b) zoomed in the contact region

cross-sectional area $A(x)/L$ are given, respectively, by

$$\frac{M(x)}{L} = \mu\frac{P}{L}(R - x) + \frac{M_0}{L} \tag{A1}$$

$$\frac{I(x)}{L} = \frac{2}{3}(R^2 - x^2)^{3/2} \tag{A2}$$

$$\frac{A(x)}{L} = 2(R^2 - x^2)^{1/2} \tag{A3}$$

According to the Timoshenko beam theory [23], the angle of rotation of the mid-surface is defined as φ. The derivative of φ is determined by $M(x)/L$ and $I(x)/L$ according to

$$\frac{M(x)}{L} = -E\frac{I(x)}{L}\frac{d\varphi}{dx} \tag{A4}$$

By integrating Eq. (A4) with the boundary condition, $\varphi = 0$ at $x = 0$, the distribution of φ is expressed as follows:

$$\varphi(x) = \frac{3}{2}\frac{\mu P}{REL}\left[\frac{R - \left(1 + \frac{M_0}{\mu RP}\right)x}{\sqrt{R^2 - x^2}} - 1\right] \tag{A5}$$

According to the Timoshenko beam theory [23], the derivative of the deflection of the half-cylinder Δ is related to φ by:

$$\frac{d\Delta}{dx} = \varphi - \frac{1}{kAG}\frac{d}{dx}\left(EI\frac{d\varphi}{dx}\right) \tag{A6}$$

By substituting $\varphi(x)$ from Eq. (A5) into Eq. (A6), the distribution of deflection of the half-cylinder Δ can be solved by integrating Eq. (A6) with the boundary condition $\Delta = 0$ at $x = 0$. The expression of $\Delta(x)$ is thus:

$$\Delta(x) = \frac{3}{2}\frac{\mu P}{EL}\left[\arcsin\left(\frac{x}{R}\right) + \left(1 + \frac{M_0}{\mu RP}\right)\frac{\sqrt{R^2 - x^2} - R}{R} - \frac{x}{R}\right]$$
$$- \frac{\mu P}{2kGL}\arcsin\left(\frac{x}{R}\right) \tag{A7}$$

The deflection of the half-cylinder at the initiation of gross slip δ_{i1} can be estimated by taking the deflection of the tip of the beam, $\delta_{i1} = \Delta(R)$. That is given by

$$\delta_{i1} = |\Delta(R)| = \left[\frac{3\mu P}{4EL}(4 - \pi) + \frac{3M_0}{2EL} + \frac{\pi\mu P}{4kGL}\right] \tag{A8}$$

Here, the Timoshenko shear coefficient k for rectangular cross section is taken according to the study by Cowper [24] as

$$k = \frac{10(1 + \nu)}{12 + 11\nu} \tag{A9}$$

and the shear modulus G is given by

$$G = \frac{E}{2(1 + \nu)} \tag{A10}$$

The influence of the moment M_0/L on δ_{i1} is now analyzed. The moment is maximum when the half-cylinder is undeformed (the curvature of the tip is maximum as if the normal load does not deform the tip of the half-cylinder). Hence, the maximum moment M_0/L can be estimated using Fig. 18. The contact region $-b < x < b$ is confined to a corresponding angle range $-\theta_0 < \theta < \theta_0$, where θ_0 is given by

$$\theta_0 = \arcsin\frac{b}{R} \tag{A11}$$

The local frictional force in this region is $q(x) = \mu p(x)$. The arm of the force is represented by the length of $\overline{OC}$ in Fig. 18 and is given by

$$\overline{OC} = 2R\sin^2\frac{\theta}{2} \tag{A12}$$

The moment on the tip of the half-cylinder M_0/L can be estimated by integrating the product of the local friction force and the arm of the
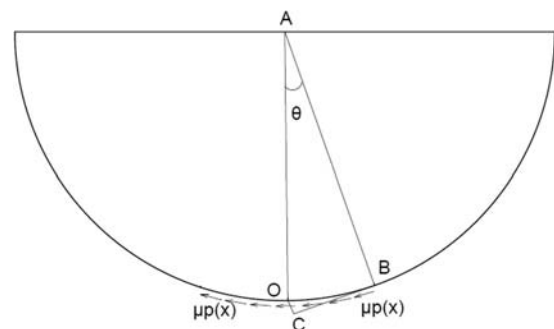
Fig. 18 The schematic of the loading condition for estimation of the moment on the tip of the half-cylinder, M_0/L

force:

$$M_0/L = \int_{-b}^{b} \mu p(x) 2R \sin^2\frac{\theta}{2} dx = \int_{-\theta_0}^{\theta_0} 2\mu p_0 \sqrt{1 - \left(\frac{R\sin\theta}{b}\right)^2} R^2 \sin^2\frac{\theta}{2} d\theta$$

$$(A13)$$

In the case where θ is small, which agrees with the conditions here ($\theta = \sim 0.01$ rad), Eq. (A13) can be simplified as follows:

$$M_0/L = \frac{\mu \pi p_0 b^3}{16R} \tag{A14}$$

According to the above estimation, the deflection of half-cylinder caused by the M_0/L is found to be less than 0.1% of the total deflection for different material cases and different normal loads with different COFs. Therefore, the moment on the tip of the half-cylinder M_0/L can largely be ignored in the foregoing.

The tangential displacement of the stick region δ_{i2} can be estimated by assuming the block to be a half elastic space and by applying the Hertzian tangential traction $q(x)$ to the surface. At the initiation of the gross slip, the local tangential traction in the contact region approaches $q(x) = \mu p(x)$ within the contact region, $[-b, b]$ (see Fig. 2), and it is given by

$$q(x) = \mu p_0 \sqrt{1 - \frac{x^2}{b^2}} \quad -b \leq x \leq b \tag{A15}$$

According to the study by Johnson [9], for a half elastic space, the derivative of the displacement on the surface of a half elastic space is determined by the distributed tangential traction.

$$\int_{-b}^{b} \frac{\mu p_0}{b} \frac{\sqrt{b^2 - s^2}}{x - s} ds = -\frac{\pi E}{2(1 - \nu^2)} \frac{du}{dx} \tag{A16}$$

The integrations of the left hand side of Eq. (A16) are distinct for the regions inside and outside the contact region, thus

$$\frac{du}{dx} = \begin{cases} -\dfrac{2(1 - \nu^2)\mu p_0}{bE}(x + \sqrt{x^2 - b^2}) & (-\infty, -b) \\ -\dfrac{2(1 - \nu^2)\mu p_0}{bE} & x(-b, b) \\ -\dfrac{2(1 - \nu^2)\mu p_0}{bE}(x - \sqrt{x^2 - b^2}) & (b, +\infty) \end{cases} \tag{A17}$$

Consequently, the tangential displacement on the surface u can be obtained by integrating Eq. (A17). Here, we take the initial center of the contact as the datum, i.e., $u(0) = 0$. Then, $u(x)$ can be derived to give

$$u = \begin{cases} -\dfrac{(1 - \nu^2)\mu p_0}{bE}\left(x^2 + x\sqrt{x^2 - b^2} - b^2 \ln\dfrac{-x - \sqrt{x^2 - b^2}}{b}\right) & (-\infty, -b) \\ -\dfrac{(1 - \nu^2)\mu p_0}{bE} x^2 & (-b, b) \\ -\dfrac{(1 - \nu^2)\mu p_0}{bE}\left(x^2 - x\sqrt{x^2 - b^2} + b^2 \ln\dfrac{x + \sqrt{x^2 - b^2}}{b}\right) & (b, +\infty) \end{cases}$$

$$(A18)$$

Note the similitude of Eq. (A18) for $(-b, b)$ and Eq. (15). The displacement of the stick region δ_{i2} at the initiation of the gross slip can be estimated by taking the difference between

the $u(x)$ at the leftmost position ($x = -2R$) and the center of the contact ($x = 0$). Thus, the estimation of δ_{i2} is $\delta_{i2} = u(0) = -u(-2R)$, giving

$$\delta_{i2} = \frac{(1 - \nu^2)\mu p_0}{bE}\left(4R^2 - 2R\sqrt{4R^2 - b^2} - b^2 \ln\frac{2R - \sqrt{4R^2 - b^2}}{b}\right)$$

$$(A19)$$

If the contact width is much smaller than the radius, $b \ll R$, Eq. (A19) can be approximated while also using Eq. (2) for p_0 to finally result in

$$\delta_{i2} = \frac{(1 - \nu^2)\mu P}{\pi EL}\left(1 - 2\ln\frac{b}{4R}\right) \tag{A20}$$

This result shows a linear relation with respect to μ and a nearly linear with respect to P/L (the nonlinearity is caused by the term $\ln(b/4R)$, where by Eq. (3), b is a function of P/L).

References

[1] Vingsbo, O., and Söderberg, S., 1988, "On Fretting Maps," Wear, **126**(2), pp. 131–147.
[2] Varenberg, M., Etsion, I., and Halperin, G., 2004, "Slip Index: A New Unified Approach to Fretting," Tribol. Lett., **17**(3), pp. 569–573.
[3] Tabor, D., 1959, "Junction Growth in Metallic Friction: The Role of Combined Stresses and Surface Contamination," Proc. R. Soc. Lond. A Math. Phys. Eng. Sci., **251**(1266), pp. 378–393.
[4] Parker, R., and Hatch, D., 1950, "The Static Coefficient of Friction and the Area of Contact," Proc. Phys. Soc. B, **63**(3), p. 185.
[5] McColl, I., Ding, J., and Leen, S., 2004, "Finite Element Simulation and Experimental Validation of Fretting Wear," Wear, **256**(11–12), pp. 1114–1127.
[6] Kim, D.-G., and Lee, Y.-Z., 2001, "Experimental Investigation on Sliding and Fretting Wear of Steam Generator Tube Materials," Wear, **250**(1–12), pp. 673–680.
[7] Zhu, M., Zhou, Z., Kapsa, P., and Vincent, L., 2001, "An Experimental Investigation on Composite Fretting Mode," Tribol. Int., **34**(11), pp. 733–738.
[8] Ahmadi, A., Sadeghi, F., and Shaffer, S., 2018, "In-Situ Friction and Fretting Wear Measurements of Inconel 617 at Elevated Temperatures," Wear, **410–411**, pp. 110–118.
[9] Johnson, K. L., 1987, Contact Mechanics, Cambridge University Press, Cambridge.
[10] Popov, V. L., and Heß, M., 2015, Method of Dimensionality Reduction in Contact Mechanics and Friction, Springer, Berlin.
[11] Kogut, L., and Etsion, I., 2002, "Elastic–Plastic Contact Analysis of a Sphere and a Rigid Flat," ASME J. Appl. Mech., **69**(5), pp. 657–662.
[12] Jackson, R. L., and Green, I., 2005, "A Finite Element Study of Elasto-Plastic Hemispherical Contact Against a Rigid Flat," ASME J. Tribol., **127**(2), pp. 343–354.
[13] Tsukizoe, T., and Hisakado, T., 1968, "On the Mechanism of Contact Between Metal Surfaces: Part 2—The Real Area and the Number of the Contact Points," J. Lubrication Technol., **90**(1), pp. 81–88.
[14] Green, I., 2005, "Poisson Ratio Effects and Critical Values in Spherical and Cylindrical Hertzian Contacts," Appl. Mech. Eng., **10**(3), pp. 451.
[15] Gupta, V., Bastias, P., Hahn, G. T., and Rubin, C. A., 1993, "Elasto-Plastic Finite-Element Analysis of 2-D Rolling-Plus-Sliding Contact With Temperature-Dependent Bearing Steel Material Properties," Wear, **169**(2), pp. 251–256.
[16] Yang, H., and Green, I., 2018, "A Fretting Finite Element Investigation of a Plane-Strain Cylindrical Contact of Inconel 617/ Incoloy 800H at Room and High Temperature," Pro IMechE Part J: J Eng. Tribol., pp. 1–17.
[17] Yang, H., and Green, I., 2018, "An Elasto-Plastic Finite Element Study of Displacement-Controlled Fretting in a Plane-Strain Cylindrical Contact," ASME Trans. J. Tribol., **140**, p. 041401.
[18] Yang, H., and Green, I., 2019, "Analysis of Displacement-Controlled Fretting Between a Hemisphere and a Flat Block in Elasto-Plastic Contacts," J. Tribol., **141**(3), p. 031401.
[19] Ghosh, A., Leonard, B., and Sadeghi, F., 2013, "A Stress Based Damage Mechanics Model to Simulate Fretting Wear of Hertzian Line Contact in Partial Slip," Wear, **307**(1), pp. 87–99.
[20] Archard, J., and Hirst, W., 1956, "The Wear of Metals Under Unlubricated Conditions," Proc. R. Soc. Lond. A, **236**(1206), pp. 397–410.
[21] Special Metals Corp., 2008, Product Handbook of High Performance Nickel Alloys, Special Metals Corp, New York.
[22] ANSYS, Inc., ANSYS®SAS IP, I., Release 17.0, Help System, Mechanical APDL Contact Technology Guide.
[23] Timoshenko, S. P., 1921, "On the Correction for Shear of the Differential Equation for Transverse Vibrations of Prismatic Bars," Lond. Edinb. Dublin Philos. Mag. J. Sci., **41**(245), pp. 744–746.
[24] Cowper, G., 1966, "The Shear Coefficient in Timoshenko's Beam Theory," J. Appl. Mech., **33**(2), pp. 335–340.